Plasma Sources Science and Technology

PAPER

Mode transition (α–γ) and hysteresis in microwave-driven low-temperature plasmas

To cite this article: Kyungtae Kim *et al* 2022 *Plasma Sources Sci. Technol.* **31** 105006

IOP Publishing

Plasma Sources Science and Technology

Plasma Sources Sci. Technol. **31** (2022) 105006 (7pp)

https://doi.org/10.1088/1361-6595/ac9331

Mode transition (α–γ) and hysteresis in microwave-driven low-temperature plasmas

Kyungtae Kim[1], Woojin Nam[2,3], Seungtaek Lee[1], Jimo Lee[1,3], Seungbo Shim[3] and Gunsu S Yun[1,2,*]

[1] Division of Advanced Nuclear Engineering, Pohang University of Science and Technology (POSTECH), Republic of Korea

[2] Department of Physics, Pohang University of Science and Technology (POSTECH), Republic of Korea

[3] Mechatronics Research, Samsung Electronics Co., Ltd, Republic of Korea

E-mail: gunsu@postech.ac.kr

Received 13 June 2022, revised 1 September 2022
Accepted for publication 20 September 2022
Published 13 October 2022

Abstract

We discovered a hysteresis in a microwave-driven low-pressure argon plasma during gas pressure change across the transition region between α and γ discharge modes. The hysteresis is manifested in that the critical pressure of mode transition depends on the direction of pressure change. As a corollary, the plasma would attain different discharge properties under the same operating parameters (pressure, power, and gas composition), suggesting a bi-stability or existence of memory effect. Analysis of the rotational and vibrational temperatures measured from the OH (A–X) line emissions shows that the hysteresis is mainly due to the fast gas heating in the γ-mode leading to a smaller neutral density than that of the α-mode. When increasing the gas pressure, the γ-mode discharge maintains a relatively higher temperature and lower neutral density, and thus, it requires a higher operating pressure to reach the α-mode. On the other hand, decreasing the pressure while maintaining α-mode, the transition to γ-mode occurs at a lower pressure than the former case due to a relatively higher neutral density of α-mode discharge. This interpretation is supported by the fact that the hysteresis disappears when the plasma properties are presented with respect to the neutral gas density instead of pressure.

Keywords: microwave-driven plasma, discharge mode transition, hysteresis, bistable state plasma, rotational temperature, fast gas heating, non-linear behavior of plasma

(Some figures may appear in colour only in the online journal)

1. Introduction

Radio-frequency sources around 10 MHz have been widely used to generate plasma discharges, owing to relatively low cost and low technical barrier [1]. Recently, with advancement in the microwave technologies, plasma sources with higher operating frequencies about 1 GHz have rapidly attracted interest from various plasma applications, such as biomaterials synthesis, polymer surface functionalization, and semiconductor fabrication [2–4], as they can produce higher electron density and higher population of energetic electrons with comparatively low power [1, 5]. In particular, microwave-driven plasmas are successfully applied to the semiconductor manufacturing processes including deposition, etching, and ashing, by varying operating parameters diversely [6–8]. Since these processes are repeatedly applied in high-precision semiconductor fabrication, it is crucial to ensure that the same plasma properties are reproduced under the same process parameters [9, 10].

Ideally, an identical plasma state would be reproduced when the external operation parameters are set to the original values as long as the discharge mode is preserved [11]. However, the

[*] Author to whom any correspondence should be addressed.

situation becomes complicated when the operation parameter space of a plasma process spans across α and γ discharge modes. Even under nominally identical operation parameters, the plasma may manifest different properties in electron and ion densities and temperatures since the electron loss and generation mechanisms change significantly crossing the discharge modes.

The discharge mechanisms of α- and γ-modes can be explained with the ionization by electron–neutral collisions and the secondary electron generation by the bombardment of fast ions to the electrode, respectively [12–16]. The representative symbols for the discharge modes, α and γ, correspond to the first Townsend avalanche coefficient in the plasma bulk and the secondary electron emission coefficient at the wall, respectively. The transition between the two modes is intuitively understood by comparing the collective oscillation amplitude of electrons and the system dimension (the electrode gap distance) [13, 14, 16–18]. The γ-mode corresponds to the situation of the oscillation amplitude being larger than the gap distance. Interestingly, particle-in-cell simulations [13] of microwave-driven atmospheric pressure plasmas showed a 'Z'-shaped frequency dependence of the gas breakdown voltage, i.e., three different breakdown voltages at the same driving frequency in the mode transition region. That observation alluded a possible existence of hysteresis when a plasma process runs in the vicinity of mode transition.

This paper reports an experimental study on low-pressure microwave-driven argon plasmas in the vicinity of mode transition, where a hysteresis is found for the change of gas pressure. Our study proposes that the nonlinear behavior of the plasma occurs due to the fast gas heating effect in γ-mode where ions are accelerated in the sheath region. This conjecture is supported by a sharp increase of rotational temperature in γ-mode, reflecting the increase of the translational temperature [19]. Furthermore, this interpretation suggests that the hysteresis may disappear by replacing the abscissa from gas pressure to neutral density, which is experimentally confirmed. It is worth noting that the origin and the detailed explanation of the hysteresis in this microwave-driven plasmas are different from those of the well-known hysteresis observed in inductively coupled plasmas during the E–H mode transition [20–22].

Our work shows that there exist bi-stable plasma states across the mode transition regime depending on the direction of pressure change. Such memory-like property of plasma in the vicinity of mode transition has an immediate implication on high-precision plasma processes where reproducible plasma states are required for high yield. A countervailing technique for the hysteresis is proposed to ensure the reproducibility of plasma state, i.e., to control the neutral density instead of the gas pressure.

2. Experiment apparatus

A coaxial transmission line resonator (CTLR) produces an electrical discharge at the open ended tip of the electrode where the resonance condition is achieved [23]. The designed resonant frequency of the electrode is about 900 MHz, where the wavelength corresponds to one-quarter of the total length of the electrode, ~83.3 mm (figure 1(a)), but due to the error and discrepancy in manufacturing, the actual resonance of the electrode appears at 890 MHz based on the S_{11} measurement by a network analyzer (E8362B, Agilent Technology). Another key parameter of the resonator design is the gap distance between inner- and outer-electrodes. In this research, the diameter of the inner electrode is about 2.8 mm and the gap distance between the electrodes is about 1.7 mm to attain a sufficiently large electric field while keeping the characteristic impedance of the device to match it with the output impedance of the power source (50 Ω).

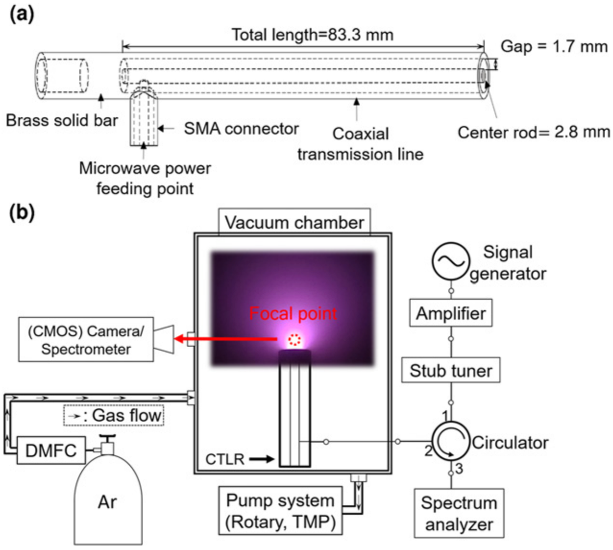

Figure 1. (a) Schematic diagram of the CTLR electrode. The microwave enters the electrode through the side port and propagates to both short- (left) and open-ended (right) sides. The wave reflected at the short end propagates to the open-end and resonates with the original microwave producing a large amplitude [23]. (b) The schematic diagram of the experimental system. The red dotted circle is the focal point of the collection optics, and its relative coordinate to the electrode is fixed throughout the entire experiment.

Figure 1(b) shows a schematic of the experimental system. The vacuum chamber was ventilated to 0.2 mTorr and filled with pure argon gas up to the pressure values of the experimental conditions around 20 mTorr. The operating pressure, which is one of the main control parameters for this experiment, was adjusted by a digital mass flow controller (DMFC, MFC KOREA). The net dissipated power by the system is preserved throughout the experiments. The incident power is maintained to 7 W. The reflected microwave is collected via a circulator and is monitored with a spectrum analyzer (E4408B, Agilent Technology) while adjusting a stub tuner to maintain its power level to less than −20 dB of the incident wave. The plasma images were taken with a high resolution CMOS camera. The optical emissions from the plasma were collected by an optical fiber and lens array focusing at the vicinity of the electrode (figure 1(b)) and analyzed using a spectrometer (USB2000, Ocean Optics).

3. Experimental results

3.1. Visual characteristics of the plasma discharges

The plasma's visible characteristics, such as volume, shape, and color, drastically change when the pressure is above or below about 20 mTorr (figure 2(a)). For a capacitive plasma, it has been reported that when the bulk size reduces and the sheath expands owing to the discharge operating parameters, the plasma becomes dominated by sheaths which can only be sustained in the so-called γ-mode. On the other hand, when the sheath is narrow and the bulk is definite, the discharge is dominated by the electrons in the plasma bulk that is called α-mode [15, 24]. This α–γ mode transition has been reported with various operating parameters [15, 24]. In microwave-driven plasmas, preceding studies explained it in terms of electron collective oscillation and electron confinement [13, 14, 17, 18]. In figure 2(b), when observing the plasma with decreasing pressure from high to low, the significant change in visibility is repeatedly observed at about 20 mTorr, which corresponds to the minimum breakdown voltage described in Paschen's curve for our plasma source [23]. Thus, we assign the critical pressure (P_c) for the α–γ mode transition to be about 20 mTorr. When $P > P_c$, the bright region of the plasma bulk is large and clear, and the sheath is spherical-shaped (confined), whereas when $P < P_c$, the bulk size reduces, and the sheath transforms into a reverse cone-shaped (scattered). Thus, we assign the discharge mode of the plasma at a higher pressure than P_c as the α-mode, and that of the plasma at a lower pressure than P_c as the γ-mode.

Interestingly, we observe the mode transitions occur at different pressures depending on the direction of the pressure change, as shown in figure 2(b). We infer that there exist two different stable states of plasma discharges that correspond to the distinct modes (α and γ) even for the same operating conditions due to the discrepancy between the critical pressures of the mode transition depending on the pathway of altering pressure. We analyze the optical emissions from the plasma to verify the cause of the hysteresis more descriptively.

3.2. Spectroscopic observations of hysteresis during α–γ mode transition

In low-pressure Ar plasmas, the intensity ratio of two line emissions, corresponding to an excited level from the ground state and another excited level from a metastable state of argon, respectively, can reveal the proportion of energetic electrons if the two levels require sufficiently different threshold energy (for impact excitation). Furthermore, it indirectly indicates the electron temperature or the change of electron temperature [25, 26]. Czerwiec and Graves [25] reported the estimation of the electron temperature using two argon line emissions with a wavelength of 750.4 nm [$3s^23p^5(^2P^o_{1/2})4p \rightarrow 3s^23p^5(^2P^o_{1/2})4s$] and 811.5 nm [$3s^23p^5(^2P^o_{3/2})4p \rightarrow 3s^23p^5(^2P^o_{3/2})4s$]. This method is utilized to analyze the proportion of energetic electrons and the change in electron temperature. Specifically, the upper level of 750.4 nm emission is mainly populated by direct excitation of the ground-state atom, and that for 811.5 nm is caused by electron impact excitation from the metastable level. The threshold energies required for these excitations are approximately 13.5 eV (750.4 nm) and 2 eV from the metastable state (811.5 nm), respectively [27]. To estimate the energetic electron population, the model comprehensively covers both changes for the metastable population and the cross-sections while the electron temperature increases [25, 26]. As a result, the line emission ratio $R_{e,e} = I_{750.4nm}/I_{811.5nm}$ is monotonically correlated with the proportion of energetic electrons. Figure 3(a) shows $R_{e,e}$ versus the operating pressure for two different directions of pressure change (increasing and decreasing).

Figure 3(a) illustrates that the proportion of energetic electrons increases rapidly when decreasing pressure below the critical pressure (P_c). Based on the numerical model of Czerwiec and Graves [25], the electron temperature is estimated to be about 2 eV for $P > P_c$ and 10 eV for $P < P_c$. The sudden increase in the electron temperature when altering the operating parameters is an evidence for the α–γ mode transition [16, 28]. Fu *et al* [11, 29] reported that the electron energy probability function evolves to a more pronounced shape in the high-energy region, generating energetic electrons during the mode transition from α to γ mode. Also, Lee *et al* [13, 14, 17] explained that such a transition in microwave-driven plasma is the discharge mode transition from the α- to γ-mode by comparing the system dimension and the collective oscillation amplitude of electrons. The experimental result (figure 3(a)) is in good agreement with the previous literature, [11, 13, 14, 16, 17, 28, 29] showing the (α–γ) discharge mode transition.

Figure 3(b) shows the drastic change in the population of argon ions during the (α–γ) mode transition. The change of ion density also influences the composition of plasma emissions from Ar I and II, and it is visible as the change in the plasma color (figure 2). The two vigorous line emissions from Ar I at 750.4 nm [$3s^23p^5(^2P^o_{1/2})4p \rightarrow 3s^23p^5(^2P^o_{1/2})4s$] and Ar II at 427.8 nm [$3s^23p^4\ (^1D)4p \rightarrow 3s^23p^4\ (^1D)4s$] are selected and compared to yield the intensity ratio $R_{Ar} = I_{427.8nm}/I_{750.4nm}$ depending on the direction of pressure change (figure 3(b)). The relative intensity of Ar II line emission increases rapidly when lowering the pressure below the $P_c \sim 20$ mTorr, implying an increase in argon ion population. The increase in the ion population is explained by the increase in the ionization rate due to the electron temperature boost during the α–γ transition. Therefore, the generation of secondary electrons by ion bombardments (γ process) becomes dominant, achieving the so-called γ-mode.

The experimental results including the visual change of plasma plumes (figure 2) and line emission ratios (figures 3(a) and (b)) clearly show the hysteresis across the transition pressure depending on the direction of pressure change. The hysteresis allows the plasma to have bi-stable states with different plasma properties under the same operating conditions depending on the pathway of operating pressure. For industrial applications such as a high precision nano-fabrication, the hysteresis may degrade the reproducibility of the plasma state and result in the loss of high yield.

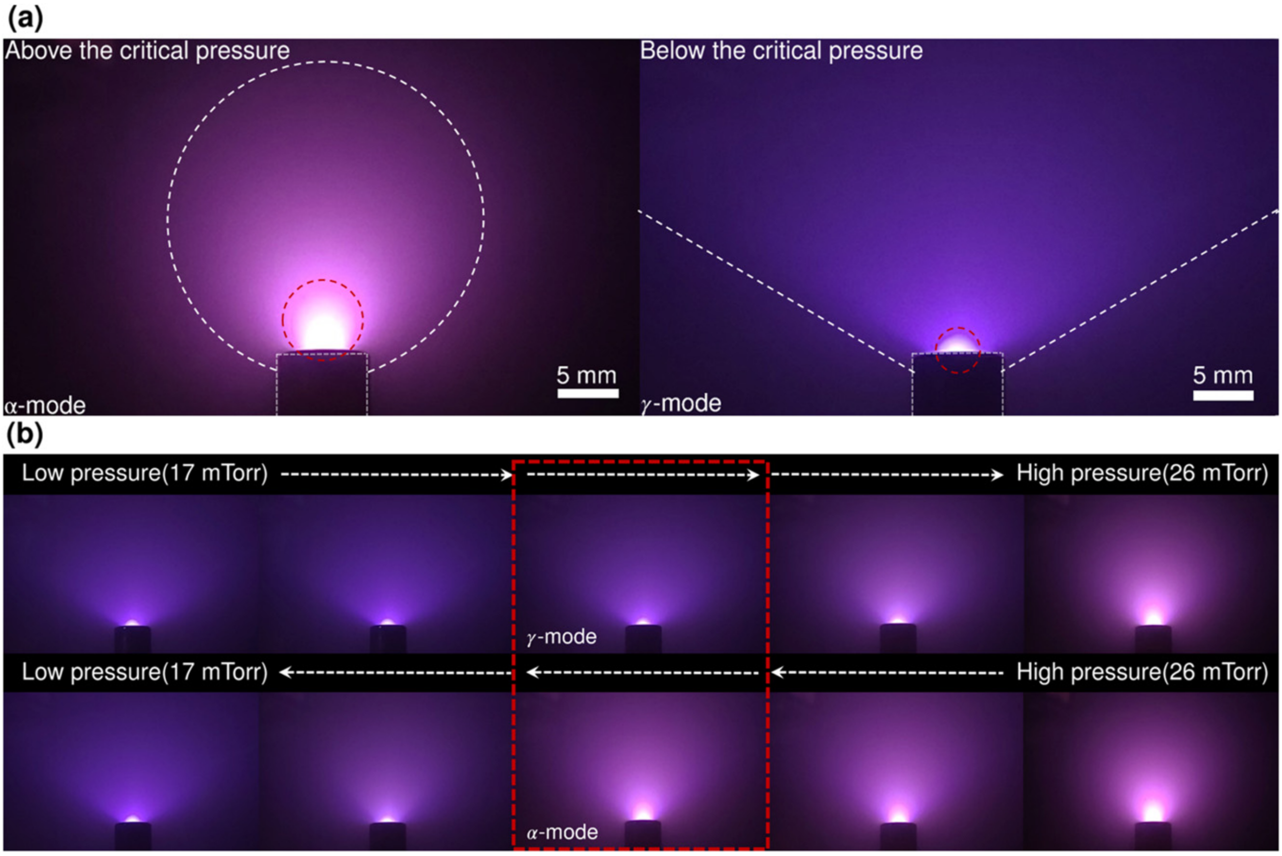

Figure 2. (a) Plasma images in two different regimes: 'α-mode' (left) and 'γ-mode' (right), when the neutral gas pressure is above the critical pressure, and below the critical pressure, respectively. (b) Visual change of the plasma when elevating pressure (top) and when lowering pressure (bottom). These snapshots show the hysteresis in the process of mode transition. The images in the center clearly exhibit different visuals that indicate different states under the same operating pressure.

3.3. The disappearance of hysteresis when data displayed to density

A rich population of argon ions in γ-mode suggests a possible explanation for the origin of the hysteresis. When the number of ions increases which have comparable masses to neutrals, it has been reported that the energy transfer rate to neutral particles accelerates due to the fast gas heating mechanism through the collisions among heavy species [30–34]. We expect the fast gas heating would occur in the γ-mode, and therefore, the neutral gas temperature of the plasma escalates during the transition from α- to γ-mode. Since the neutral density is the key parameter to determine the collective oscillation amplitude of electrons, the preservation of small neutral density in γ-mode results in the shift of P_c to a higher pressure during the increase of the operating pressure. Consequently, to achieve the transition from γ- to α-mode which requires a smaller oscillation amplitude of electrons, the operating pressure should reach further.

This explanation is verified by the fact that the hysteresis in the spectroscopic data disappear when they are displayed to density, not pressure. Figures 3(c) and (d) show the line emission ratios versus gas density and the disappearance of hysteresis between the experimental cases, increasing and decreasing the operating pressure. The disappearance of hysteresis suggests a method of avoiding the non-linear behavior or bi-stability of the plasma states, that is, to monitor the neutral density while controlling the operating parameters. In particular, the method is a convenient way of improving and ensuring the reproducibility of the processing plasmas for nano-fabrication, such as high-precision semiconductors.

The equation of state for an ideal gas, $P = nk_BT$ is assumed where k_B and T are the Boltzmann constant and temperature of the argon gas, respectively. This assumption is relevant since the pressure is sufficiently low whereas the gas temperature is high enough [35], which leads the gas density to be the pressure divided by the temperature. Additionally, in this experiment, the gas temperature is considered to be in the same order as the rotational temperature of the hydroxyl radical (OH) contained in the gas for a diagnostic purpose within a reasonable error of about 10% [19, 36, 37]. A practical advantage of this method to monitor the gas density for avoiding hysteresis is that there is no need for an extra measurement system but an optical spectrometer.

3.4. The hysteresis in the rotational and vibrational temperatures

The base vacuum pressure is approximately 1% of the experimental pressure (∼30 mTorr), and thus the plasma contains impurities such as hydroxyl radicals (OH) which originate from the water vapor on the wall of the vacuum chamber. The

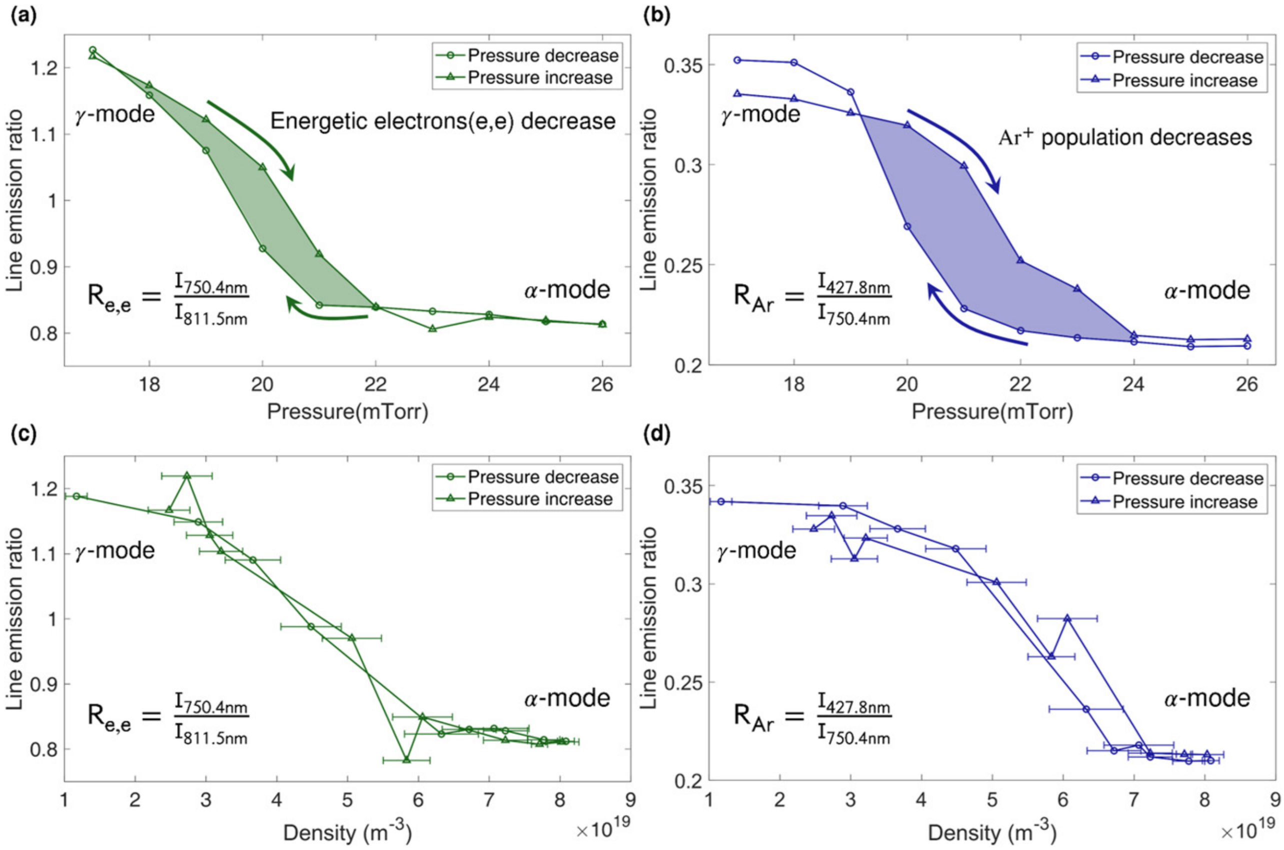

Figure 3. (a) Line emission ratio ($R_{e,e} = I_{750.4nm}/I_{811.5nm}$) versus pressure. $R_{e,e}$ represents the proportion of energetic electrons and shows the change in electron temperature. The high proportion of energetic electrons below the critical pressure indicates the higher electron temperature. There exists a hysteresis depending on the direction of pressure change. (b) Line emission ratio ($R_{Ar} = I_{427.8nm}/I_{750.4nm}$) versus pressure. R_{Ar} represents the population of argon ion. There also exists a hysteresis in the ratio R_{Ar} depending on the direction of pressure change. (c) and (d) Line emission ratios ($R_{e,e}, R_{Ar}$) versus density; operating pressure divided by the rotational temperature measured by analyzing OH line emissions. The hysteresis for both ratios disappear when they are displayed to neutral density.

line emissions from the trace amount of OH molecules are employed to measure the rotational and vibrational temperatures by fitting them with the LIFBASE simulation [38–41]. As the experimental resolution is about 0.6 ± 0.3 nm, the line emissions are compared with the simulation data that are relatively filtered, and the best fit gives the temperature estimation for a given pressure with a maximum error of about 15%.

Figure 4(a) illustrate that OH(A–X) line emissions are in good agreement with the data from the LIFBASE simulation. The OH line emissions are classified into the three distinctive groups; the R and P branches centered at 307 nm and 309 nm, respectively, and a tail ranging from 310 nm to 320 nm. The rotational temperature is generally determined by the intensity ratio between the two branches [38]. On the other hand, the vibrational temperature mostly correlates with the shape of the tail structure.

Figure 4(b) shows the rotational and vibrational temperatures estimated from the OH line emissions for both experimental conditions of increasing and decreasing the operating pressure. Both temperatures present the hysterical trends to the operating pressure but in the opposite fashion. The rotational temperature increases during the mode transition from γ to α while the vibrational temperature does for α to γ. The behavior of vibrational temperature, which is opposite to the other measurements (rotational temperature, electron temperature, and ion population), will be discussed shortly. As we expected, the rotational temperature, which is a good approximation of the gas temperature, manifests a hysteric trend over the pressure alteration, and thus, the non-linear behavior of rotational temperature resolves the hysteresis in the other measurements, such as the electron temperature and the ion population (figures 3(c) and (d)).

A steady-state plasma model can explain the trend of vibrational temperature. Zheng-De and Yi-Kang reported a rapid increase in the vibrational temperature along with the pressure change for the low-pressure plasmas, and explained the phenomenon with a simplified model under the following assumptions: (1) the excited state is generated only by the electron impact excitation from the ground-state. (2) The Franck–Condon principle is applicable to these excitation transitions. (3) The collisional de-excitation process is negligible and introduces a Boltzmann distribution for all vibrational levels of molecules to be measured [42]. For a steady-state plasma, the vibrational temperature is expressed as

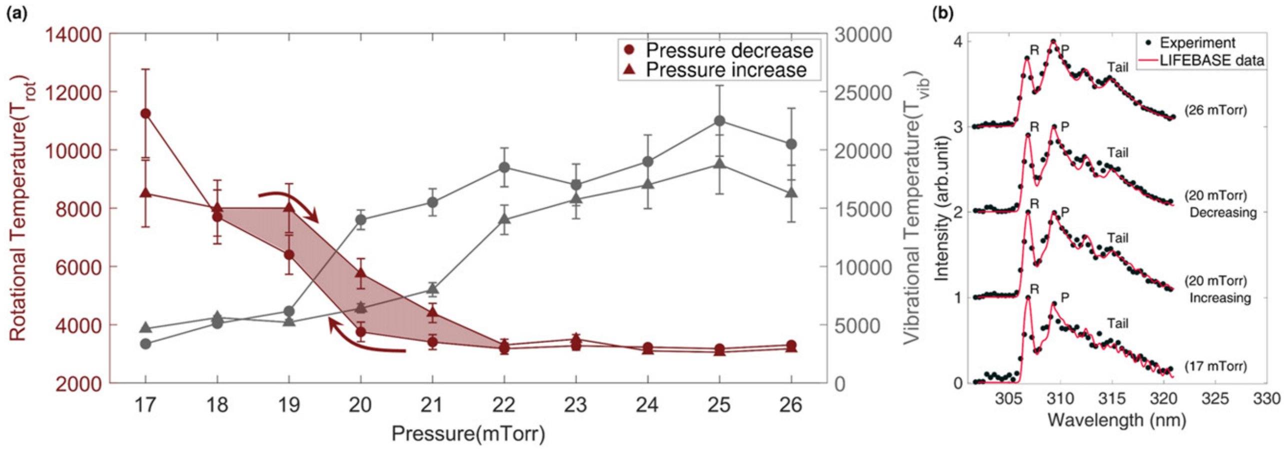

Figure 4. The rotational and vibrational temperatures from the OH line emissions. (a) The rotational and vibrational temperatures versus pressure. The circular and triangular markers correspond to the experimental conditions of decreasing and increasing the operating pressures, respectively. The hysteresis are observed in both molecular temperatures but in the opposite fashion. The rotational temperature increases when the pressure is low, but the vibrational temperature has an opposite trend. (b) The OH(A–X) line emissions and their fit with the LIFBASE simulations for the selected pressures.

$$T_{\rm vib} = \left(\frac{E_{\rm vib}}{k_{\rm B}}\right)\left[\ln\left\{\frac{n_0}{n_{\rm e}n_{\rm g}K_{\rm vib}\tau}\right\}\right]^{-1} = \left(\frac{E_{\rm vib}}{k_{\rm B}}\right)\frac{1}{C-\ln K_{\rm vib}}, \tag{1}$$

where $T_{\rm vib}$ is the vibrational temperature, $E_{\rm vib}$ is the vibrational state energy, $n_{\rm e}$ is the electron density, $n_{\rm g}$ is the background gas density, $K_{\rm vib}$ is the rate coefficient for the vibrational excitation as a function of electron temperature, τ is the timescale to reach steady-state, and $C \equiv \ln(n_0/n_{\rm e}n_{\rm g}\tau)$.

The model has been compared with the experiments covering a broad range of pressure and applies to the OH(A–X) line emissions around near-UV under the assumption that the electron impact excitation is the dominant process for the transition from the ground to the first excited states of OH molecules. The vibrational temperature is positively correlated to the rate coefficient $K_{\rm vib}$ under the given parameters (n_0, $n_{\rm e}$, $n_{\rm g}$, τ, and $E_{\rm vib}$), through the equation (1).

The rate coefficient $K_{\rm vib}$ generally follows a form of the Arrhenius equation, and for the OH molecule, it exponentially decreases above $\sim$1 eV [43–45], and thus, the vibrational temperature is strongly affected by the electron temperature compared to other factors. As a result, when the electron temperature increases in the γ-mode, the vibrational temperature decreases. Based on the steady-state model, the hysteresis observed in the vibrational temperature (figure 4(b)) is explained to have an opposite trend to other plasma parameters such as electron temperature, ion population, and rotational temperature.

4. Conclusion

We found hysteresis in microwave-driven low-temperature plasma across the discharge mode transition (α–γ). This observation suggests that plasma under the same operating parameters can have two different stable states. We have identified the discharge mode transition at the critical pressure ($\sim$20 mTorr) occurs by observing the visual characteristics of the plasma and two separate plasma properties related to the electron kinetics that depend on the neutral particle density and the electron temperature: the ratio of two emission peaks from different excitation processes.

The hysteresis across the discharge mode transition is explained by the increase of the ion population in the γ-mode, and numerous fast ions provoke the fast gas heating. Owing to the fast gas heating in the γ-mode, the neutral density of the γ-mode stays smaller than that of the α-mode, and the amplitude of the collective electron oscillation in the γ-mode becomes larger than that of the α-mode. As a result, a higher critical pressure is required for the γ to α transition when the system pressure increases, compared to the case of the α to γ transition when the system pressure decreases.

In conclusion, the difference in the gas density of the plasma under the same global operating parameters allows the plasma to have bi-stable states with different plasma properties. We suggest that the bi-stability of the plasma in the vicinity of the mode transition may cause unexpected problems in the high-precision plasma processes where the reproducibility of the plasma properties is essential while varying the global operating parameters repetitively. Furthermore, we propose a simple and cost-efficient method of avoiding the hysteresis by monitoring the neutral density along with the operating pressure.

Acknowledgments

This work was supported by Samsung Electronics Co., Ltd (Grant No. IO201209-07922-01) and the National Research Foundation of Korea (NRF) (BK21 FOUR program).

Data availability statement

The data that support the findings of this study are available upon reasonable request from the authors

ORCID iDs

Kyungtae Kim https://orcid.org/0000-0002-0553-3637
Woojin Nam https://orcid.org/0000-0002-2124-4122
Seungtaek Lee https://orcid.org/0000-0002-3292-4967
Jimo Lee https://orcid.org/0000-0001-7019-9279
Gunsu S Yun https://orcid.org/0000-0002-1880-5865

References

[1] Moisan M, Barbeau C, Claude R, Ferreira C M, Margot J, Paraszczak J, Sá A B, Sauvé G and Wertheimer M R 1991 *J. Vac. Sci. Technol.* B **9** 8
[2] Musil J 1986 *Vacuum* **36** 161
[3] Vesel A and Mozetic M 2017 *J. Phys. D: Appl. Phys.* **50** 293001
[4] Förch R, Zhang Z and Knoll W 2005 *Plasma Process. Polym.* **2** 351
[5] Lebedev Y A 2015 *Plasma Sources Sci. Technol.* **24** 053001
[6] Donnelly V M and Kornblit A 2013 *J. Vac. Sci. Technol.* A **31** 050825
[7] Bera M, Mahata C and Maiti C 2008 *Thin Solid Films* **517** 27
[8] Bera M and Maiti C 2008 *Microelectron. Reliab.* **48** 682
[9] Şengül H, Theis T L and Ghosh S 2008 *J. Ind. Ecol.* **12** 329
[10] Graves D B 1994 *IEEE Trans. Plasma Sci.* **22** 31
[11] Fu Y, Zheng B, Zhang P, Fan Q H, Verboncoeur J P and Wang X 2020 *Phys. Plasmas* **27** 113501
[12] Godyak V, Piejak R and Alexandrovich B 1992 *Phys. Rev. Lett.* **68** 40
[13] Lee M U, Lee J, Lee J K and Yun G S 2017 *Plasma Sources Sci. Technol.* **26** 034003
[14] Lee M U, Lee J, Yun G S and Lee J K 2017 *Eur. Phys. J.* D **71** 94
[15] Shi J and Kong M 2006 *Phys. Rev. Lett.* **96** 105009
[16] Iza F, Kim G J, Lee S M, Lee J K, Walsh J L, Zhang Y T and Kong M G 2008 *Plasma Process. Polym.* **5** 322
[17] Lee M U, Lee J K and Yun G S 2018 *Plasma Process. Polym.* **15** 1700124
[18] Kihara T 1952 *Rev. Mod. Phys.* **24** 45
[19] Lavrov B P and Otorbaev D K 1978 *Sov. Tech. Phys. Lett.* **4** 574
[20] Lee H-C, Kim D-H and Chung C-W 2013 *Appl. Phys. Lett.* **102** 234104
[21] Lee H-C and Chung C-W 2015 *Sci. Rep.* **5** 15254
[22] Baële P, Béchu S, Bès A, Pelletier J and Lacoste A 2014 *Plasma Sources Sci. Technol.* **23** 064006
[23] Choi J, Iza F, Do H, Lee J and Cho M 2009 *Plasma Sources Sci. Technol.* **18** 025029
[24] Liu D, Iza F and Kong M G 2009 *Appl. Phys. Lett.* **95** 031501
[25] Czerwiec T and Graves D 2004 *J. Phys. D: Appl. Phys.* **37** 2827
[26] Boffard J B, Lin C C and Wendt A E 2018 *Advances in Atomic, Molecular, and Optical Physics* vol 67 (Amsterdam: Elsevier) pp 1–76
[27] Dünnbier M, Becker M, Iseni S, Bansemer R, Loffhagen D, Reuter S and Weltmann K 2015 *Plasma Sources Sci. Technol.* **24** 065018
[28] Abdel-Fattah E and Farag O F 2013 *Can. J. Phys.* **91** 1062
[29] Fu Y, Zheng B, Wen D-Q, Zhang P, Fan Q H and Verboncoeur J P 2020 *Appl. Phys. Lett.* **117** 204101
[30] Popov N 2011 *J. Phys. D: Appl. Phys.* **44** 285201
[31] Lee H-C, Seo B, Kwon D-C, Kim J, Seong D, Oh S, Chung C-W, You K and Shin C 2017 *Appl. Phys. Lett.* **110** 014106
[32] Doyle S J, Gibson A R, Flatt J, Ho T S, Boswell R W, Charles C, Tian P, Kushner M J and Dedrick J 2018 *Plasma Sources Sci. Technol.* **27** 085011
[33] Shi J and Kong M 2005 *J. Appl. Phys.* **97** 023306
[34] Bellan P M 2008 *Fundamentals of Plasma Physics* (Cambridge: Cambridge University Press)
[35] Tenny K M and Cooper J S 2017 *Ideal Gas Behavior* (Treasure Island, FL, USA: StatPearls Publishing)
[36] Bruggeman P, Sadeghi N, Schram D and Linss V 2014 *Plasma Sources Sci. Technol.* **23** 023001
[37] Osiac M, Lavrov B and Röpcke J 2002 *J. Quant. Spectrosc. Radiat. Transfer* **74** 471
[38] Laux C O, Spence T, Kruger C and Zare R 2003 *Plasma Sources Sci. Technol.* **12** 125
[39] Luque J and Crosley D R 1999 Lifbase: Database and spectral simulation program (version 1.5) *SRI International Report MP 99*
[40] Meng Y, Gu H and Chen F 2022 *Aerospace* **9** 73
[41] Parigger C G, Helstern C M, Jordan B S, Surmick D M and Splinter R 2020 *Molecules* **25** 988
[42] Zheng-De K and Yi-Kang P 2002 *Chin. Phys. Lett.* **19** 211
[43] Lieberman M A and Lichtenberg A J 2005 *Principles of Plasma Discharges and Materials Processing* (New York: Wiley)
[44] Campbell L and Brunger M J 2018 *Planet. Space Sci.* **151** 11
[45] Brunger M J and Buckman S J 2002 *Phys. Rep.* **357** 215